Research Article

Simultaneous creation of multiple vortex-antivortex pairs in momentum space in photonic lattices

Feng Li[a], Sergei V. Koniakhin,[b,c,*] Anton V. Nalitov,[d,e,f] Evgeniia Cherotchenko,[g] Dmitry D. Solnyshkov[h,i] Guillaume Malpuech,[h] Min Xiao,[j,k] Yanpeng Zhang,[a] and Zhaoyang Zhang[a,*]

[a]Xi'an Jiaotong University, Key Laboratory for Physical Electronics and Devices of the Ministry of Education, Shaanxi Key Laboratory of Information Photonic Technique, School of Electronic Science and Engineering, Faculty of Electronics and Information, Xi'an, China
[b]Institute for Basic Science, Center for Theoretical Physics of Complex Systems, Daejeon, Republic of Korea
[c]Korea University of Science and Technology (UST), Basic Science Program, Daejeon, Republic of Korea
[d]Moscow Institute of Physics and Technology, Dolgoprudnyi, Russia
[e]University of Wolverhampton, Faculty of Science and Engineering, Wolverhampton, United Kingdom
[f]ITMO University, St. Petersburg, Russia
[g]Ioffe Institute, St. Petersburg, Russia
[h]Université Clermont Auvergne, Institut Pascal, PHOTON-N2, CNRS, Clermont INP, Clermont-Ferrand, France
[i]Institut Universitaire de France, Paris, France
[j]University of Arkansas, Department of Physics, Fayetteville, Arkansas, United States
[k]Nanjing University, School of Physics, National Laboratory of Solid State Microstructures, Nanjing, China

Abstract. Engineering of the orbital angular momentum (OAM) of light due to interaction with photonic lattices reveals rich physics and motivates potential applications. We report the experimental creation of regularly distributed quantized vortex arrays in momentum space by probing the honeycomb and hexagonal photonic lattices with a single focused Gaussian beam. For the honeycomb lattice, the vortices are associated with Dirac points. However, we show that the resulting spatial patterns of vortices are strongly defined by the symmetry of the wave packet evolving in the photonic lattices and not by their topological properties. Our findings reveal the underlying physics by connecting the symmetry and OAM conversion and provide a simple and efficient method to create regularly distributed multiple vortices from unstructured light.

Keywords: vortex; photonic lattice; orbital angular momentum; topology; symmetry.

1 Introduction

A vortex is a fundamental topological structure associated with the circulation loops in various vector fields. Quantized vortices present in quantum fluids were discovered as elementary topologically nontrivial excitations of superfluid helium[1] and superconductors.[2] In scalar quantum fields, the existence of vortices is allowed by the gauge invariance of the wave functions (WFs) with respect to phase shifts of $2\pi n$ ($n \in \mathbf{Z}$). The phase ambiguity at the vortex core requires a vanishing WF

density, which is a vivid observable signature. Another manifestation is a diverging momentum curl, which results in non-vanishing energy and angular momentum contributions associated with the vortex. Importantly, in many-body systems of interacting particles, described with the Gross–Pitaevskii equation, quantum vortices are stable solutions whose spatio-temporal dynamics governs the quantum turbulence.[3–6] Stable and well-defined quantum vortices are also present in driven-dissipative systems, such as exciton–polariton interacting quantum fluids,[7–10] where they are responsible for the Berezinskii–Kosterlitz–Thouless transition.[11] The polaritonic spin-orbit coupling due to the TE-TM splitting [12,13] allows new topologically nontrivial excitations such as half-integer

vortices[14] and polarization vortices[15] in semiconductor microcavities.

Along with the real space vortices, similar topological configurations exist in reciprocal (momentum) space. Such vortices may stem from the nontrivial topology in band structures, manifesting Berry curvature sources. In graphene, momentum space vortices of the eigenstates induced by pseudospin exist at Dirac points[16–18], and their topological charges have opposite signs in the two non-equivalent valleys in the valence and conduction bands. In general, pseudospin (sublattice) and valley (K and K') degrees of freedom lead to rich optical behaviors in artificial graphene and related photonic lattices for orbital angular momentum (OAM) managing. In photonic honeycomb and Lieb lattices, pseudospin-orbit interaction allowed obtaining the conversion of pseudospin and OAM[19] into the angular momentum of the output signal. At the same time, valley-selective excitation by a structured field in photonic graphene leads to the emergence of vortices of topological charge with arbitrary sign in the Bragg-reflected component in the complementary Dirac points.[20] Polarization vortices in momentum space were reported in topological honeycomb and Lieb plasmonic lattices,[21] and their conversion into real-space vortices was shown for bound states in the continuum.[22] The strong spin-orbit coupling was employed to give rise to the appearance of spin antivortices in momentum space in atomically thin metals with graphene-like structure.[23] The relation and the interconversion of real and reciprocal space vortices offer large possibilities for beam engineering with broad applications.[24–27]

Recently, the artificial photonic lattices based on coherent atomic vapors with refraction index modulated by electromagnetically induced transparency (EIT)[28] have shown their advantages for analog physics: the real-time tuning of the lattice potential that allows for studying the dynamics of the wave packets. This technique boosted the investigation and visualization of angle-dependent Klein tunneling[29] and edge-state solitons,[30] as well as the observation of particle-like dynamics of the vortex cores formed during the wave packet evolution in photonic graphene.[31] So far, the conversion between OAM and the pseudospin via the Dirac point involved complicated beam structures to ensure the excitation of a single pseudospin of the lattice, which generates one specific vortex corresponding to the excited pseudospin.[20,31–33] Therefore, it is essential to find alternative mechanisms for creating vortices with simpler schemes, better efficiency, and richer physics. Meanwhile, as all the above-mentioned systems involve geometrically symmetric lattices that display topological features, it is not clear whether topology is a necessity for the generation of vortices, or whether the vortices simply originate from the lattice symmetry.

In this article, we report the creation of momentum space vortices in atomic-vapor-cell-based honeycomb and hexagonal photonic lattices excited by a nonstructured Gaussian probe beam. Such a scheme allows the easy generation of multiple vortex-antivortex pairs uniformly distributed in momentum space upon a single excitation. Moreover, the resulting OAM textures can be tuned via probe symmetry. Our study reveals the underlying physics between symmetry and vortex generation and shows that such processes are possible even in the absence of any Berry curvature.

2 Materials and Methods

The photonic lattice is created by engineering the susceptibility via the EIT effect in a ^{85}Rb vapor cell.[28,31] As sketched in Fig. 1(a), the coupling field E_2 is constructed by the interference of three light beams from the same laser, forming a two-dimensional (2D) hexagonal pattern in the $x-y$ plane propagating along z. For simplicity, the optical path of E_2 is not shown in the graph, with technical details already introduced in Ref. 31. The probe beam E_1 from a second laser, focused by a lens onto the front surface of the atomic vapor cell, propagates through the cell and experiences variation of susceptibility of the medium induced by coupling field E_2. Then it is collected by another lens with the same focal length and detected by a charge coupled device (CCD) camera placed at the collection lens' back focal plane, which shows the Fourier image presenting the momentum space of the probe beam. The phase measurements are made by homodyne detection, i.e., by interfering the probe beam with a reference beam from the same laser at the position of the CCD, where the fork-like structure of the interference stripes indicates the formation of vortices. The susceptibility experienced by E_1 is determined by the frequency detunings of E_1 (denoted as Δ_1) and E_2 (denoted as Δ_2) via the EIT effect in a three-level atomic configuration [Fig. 1(b)]. When the two-photon detuning Δ_1-Δ_2 is set to result in higher (lower) refractive index at the bright sites of the hexagonal pattern, the bright (dark) sites form a hexagonal (honeycomb) photonic lattice. Figures 1(c) and 1(d) show the simulated spatial distribution of the refractive indices of the honeycomb and hexagonal lattices, respectively. The Gaussian probe beam is focused to a spot size comparable to that of a honeycomb lattice site. During the propagation along z in the 2D lattice, which can be considered as a matrix of coupled waveguides, the probe beam expands within the $x-y$ plane and interacts with the 2D lattice to form reciprocal space vortices. It should be noted that the coupling field E_2 alone induces the EIT effect, but does not allow one to observe and utilize it. This is why we send the probe beam, and we study its evolution under the EIT conditions. However, when performing the measurements with a coupling field only, one observes maxima at three equivalent K points of the induced honeycomb lattice, which allows one to locate the positions of vortices in momentum space in the configuration with probe beam E_1 in further experiments; see Fig. S1 in the Supplementary Material.
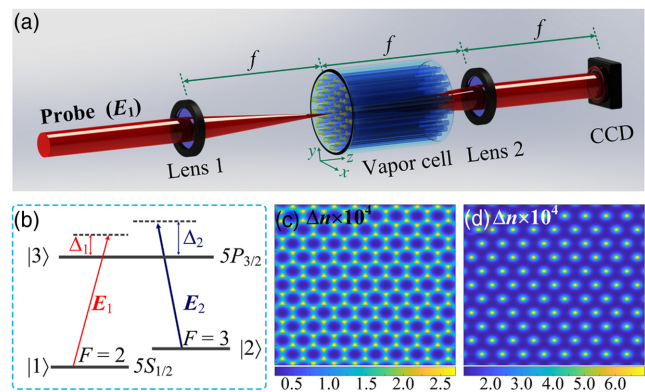

Fig. 1 Experimental schemes. (a) Illustrative picture of the experimental setup. The focus lengths of the two lenses are both $f = 150$ mm. (b) The three-level ^{85}Rb atomic configuration excited by the probe field E_1 and the hexagonal coupling field E_2. (c) and (d) Calculated spatial distribution of refractive index for $\Delta_1 = -80$ MHz (c) and $\Delta_1 = -190$ MHz (d) with $\Delta_2 = -100$ MHz, resulting in honeycomb and hexagonal lattices, respectively.

3 Results

We first set the frequency detunings as $\Delta_1 = -80$ MHz and $\Delta_2 = -100$ MHz, which yields a honeycomb lattice in the Rb cell with a lattice constant of ~ 76 μm, as shown in Fig. 1(c). The probe beam is centered at one of the honeycomb lattice sites. After propagating through the Rb cell, the interference pattern between the momentum space image and the reference beam shows six evenly distributed fork-like features in the interference fringes, indicating the presence of six vortices, as shown in Figs. 2(a) and 2(b). The vortices are located near the Dirac points, and their signs depend on the neighboring valley type, K or K'. The probe beam, which is focused to a small spot, contains a large range of incident angles (determined by the lens numerical aperture) that correspond to a continuum of photon momenta. The intensity of the high-momentum probe components is enough to excite sufficiently not only the first Brillouin zone (BZ), but also its nearest replicas (reciprocal lattice cells) and thus to generate well-resolved vortices near the Dirac points in momentum space, providing an easy technology of generating multiple and spatially well-separated vortices using nonstructured light.

Although the vortices can be originated from the Berry curvature sources associated with the Dirac points, as previously reported,[19] such an interpretation does not apply to our configuration. Instead, we find that creation of multiple vortices is very sensitive to the initial position of the focused probe beam on the honeycomb lattice, indicating that the process occurs only under special situations highly restricted by symmetry. This indicates that the vortex formation in such systems is strongly associated with the symmetry of the excited wave packet and the properties of Fourier transformation of the finite size signals in periodic lattices.

To perform a quantitative theoretical analysis of the beam propagation in the photonic graphene lattice, we have used the paraxial approximation for the probe field profile in the vapor cell with spatial modulation of the refraction index, equivalent to Schrödinger equation with the honeycomb-type potential with the correspondence between the z coordinate in the cell and time.[31] Emergence of the momentum space quantized vortices was reproduced with the initial WF state defined as a narrow Gaussian profile with a width comparable to the size of a single site. It was centered on one of the honeycomb lattice sites, as in experiment. The details of calculations, including initial

conditions are given in the Supplementary Material. In this excitation configuration, the real space WF of the probe beam exhibits a C_{3v} symmetry during time evolution, as shown in Fig. 3(a). The calculated momentum space profiles, as depicted in Figs. 3(b)–3(d) for the probability density, phase, and interference patterns, show the quantum vortices in the vicinity of the Dirac points, robustly determined by the automatic vortex detection algorithm.[6] These results agree very well with the experimental measurements. The real part of the WF Fourier image (as well as its absolute value) has a sixfold rotation symmetry, whereas the imaginary part obeys the C_{3v} symmetry, in accordance with Refs. 34–36. This result is similar to the one given in Fig. 1(a) from Ref. 34 with the exchanged real and momentum space.

The time-dependent tight-binding-type model (TBM) calculations ascertain insensitivity of the results to the particular shape of the site potential. The initial condition with a single excited site was used, which corresponds to the numerical solution of the full Schrödinger equation and the experimental design. Figure 3(e) shows the probability density in real space, and Fig. 3(f) depicts the interference pattern in momentum space with better visible BZ replicas.

The 2D Fourier transform $\tilde{\psi}(\mathbf{k}) = \iint \psi(\mathbf{r}) e^{-i\mathbf{k}\mathbf{r}} d\mathbf{r}$ can be evaluated analytically within the TBM in the approximation of delta function sites at the time given by inverse tunneling constant $t = \pi\hbar/J$. At this moment, WF $\psi(\mathbf{r})$ is dominantly located at the first nearest neighbors (NNs) of the initially excited site and momentum space signal has a form

$$\tilde{\psi}(\mathbf{k}) = \sum_{j=1,2,3} e^{-i\mathbf{k}\mathbf{d}_j} \equiv f(\mathbf{k}), \tag{1}$$

with $\mathbf{d}_j$ the radius-vectors of three NNs. The phase of $\tilde{\psi}(\mathbf{k})$ manifests the phase factors $\pm 2\pi/3$ in the vicinity of Γ points of BZ replicas and $\pm 2\pi$ winding (vortices) around Dirac points in the same way as demonstrated in Refs. 16 and 18 for the relative phase of the sublattices in the eigenstates of graphene TBM Hamiltonian,

$$H_{\mathbf{k}} = -J \begin{pmatrix} 0 & f_{\mathbf{k}}^+ \\ f_{\mathbf{k}} & 0 \end{pmatrix}, \tag{2}$$

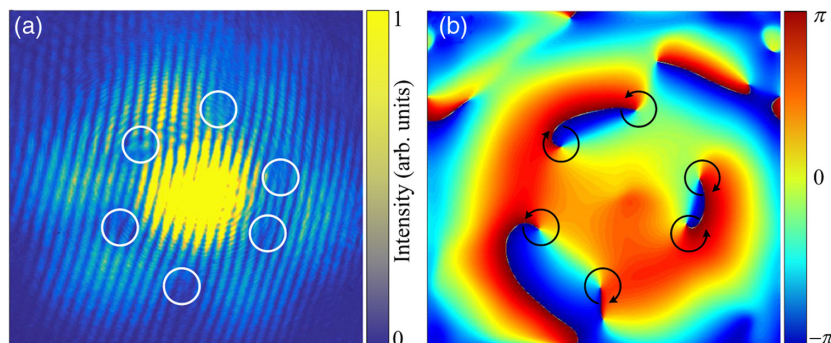which is besides defined via $f(\mathbf{k})$ in momentum representation.

Fig. 2 Momentum space vortex generation in the honeycomb lattice with the two-photon detuning being 20 MHz. (a) Experimentally measured momentum space image interference with the reference beam. The dislocations in fringes correspond to the vortices (marked by white circles). (b) The corresponding phase pattern extracted from the interference image. Black arrows show the rotation direction.
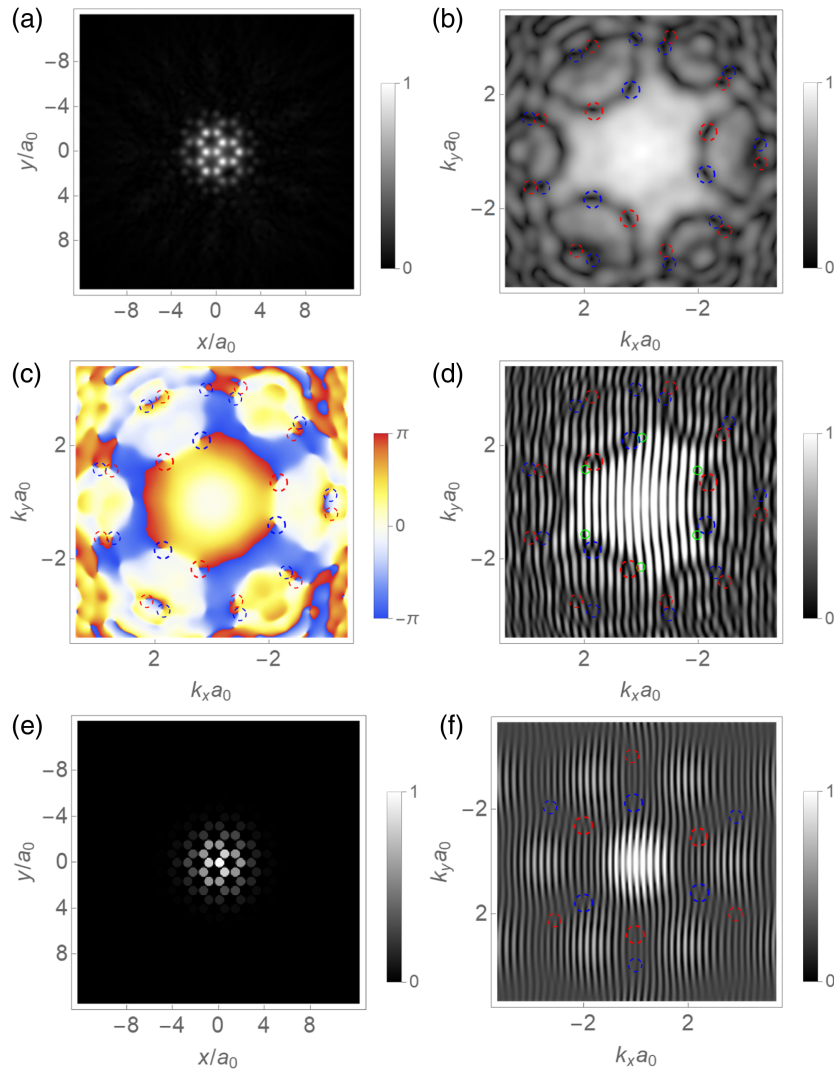
Fig. 3 Numerical solution of the Schrödinger equation showing wave packet expansion in photonic graphene starting from the excitation of a single site. (a) The probability distribution in real space. (b) The probability distribution in momentum space. (c) The reciprocal space phase image of the WF corresponding to panel (b). The left and right vortices are marked with blue and red circles, respectively. (d) The reciprocal space WF interference with a plane wave. Green circles indicate the Dirac points. The snapshot shows that the WF has the C_{3v} symmetry. Panels (e) and (f) show the results of tight-binding calculation and correspond to panels (a) and (d), respectively.

However, such direct correspondence with a tight-binding Hamiltonian is only obtained in this particular case. More generally, the Dirac point vortices exist in the basic element of the C_{3v} symmetry WF in honeycomb lattice, a tetramer, formed of one central site with $\Psi_0 = 1$ and three neighbors with $\Psi_{1,2,3} = ae^{i\varphi}$, depending on parameters a and φ; see Fig. S3 in the Supplementary Material. Qualitatively, the tunneling from the initial site or sites to their neighbors in real space leads to the accumulation of a phase for various wave vectors in agreement with the Fourier shift theorem. The gained phase difference of the momentum space points depends on the symmetry of WF in real space and leads to a nonzero winding around the Dirac points, resulting in the reciprocal space vortices we observe. According to the Fourier shift theorem, for site separation distances of the order of lattice constant a_0, the wave

vectors $\gtrsim \pi/a_0$ corresponding to higher BZ replicas, as in the performed experiments, must be involved to gain a phase difference $\sim \pi$ required to observe the vortices.

Other types of the WF symmetry that can be realized in the honeycomb lattice are the C_{6v} and C_{2v} symmetries. Figures 4(a) and 4(b) show the WF in real space and its phase in momentum space for initial excitation of six sites belonging to the same hexagon. For a C_{6v}-object, both real and imaginary parts of the momentum space WF inherit its symmetry, which forbids the presence of single opposite-signed vortices near the Dirac points due to the mirror reflection symmetry. Figures 4(c) and 4(d) demonstrate the vortices in the momentum space for initial excitation between two NN sites. In this case, the vortices in momentum space are positioned at the rectangle corners in agreement with C_{2v} symmetry.
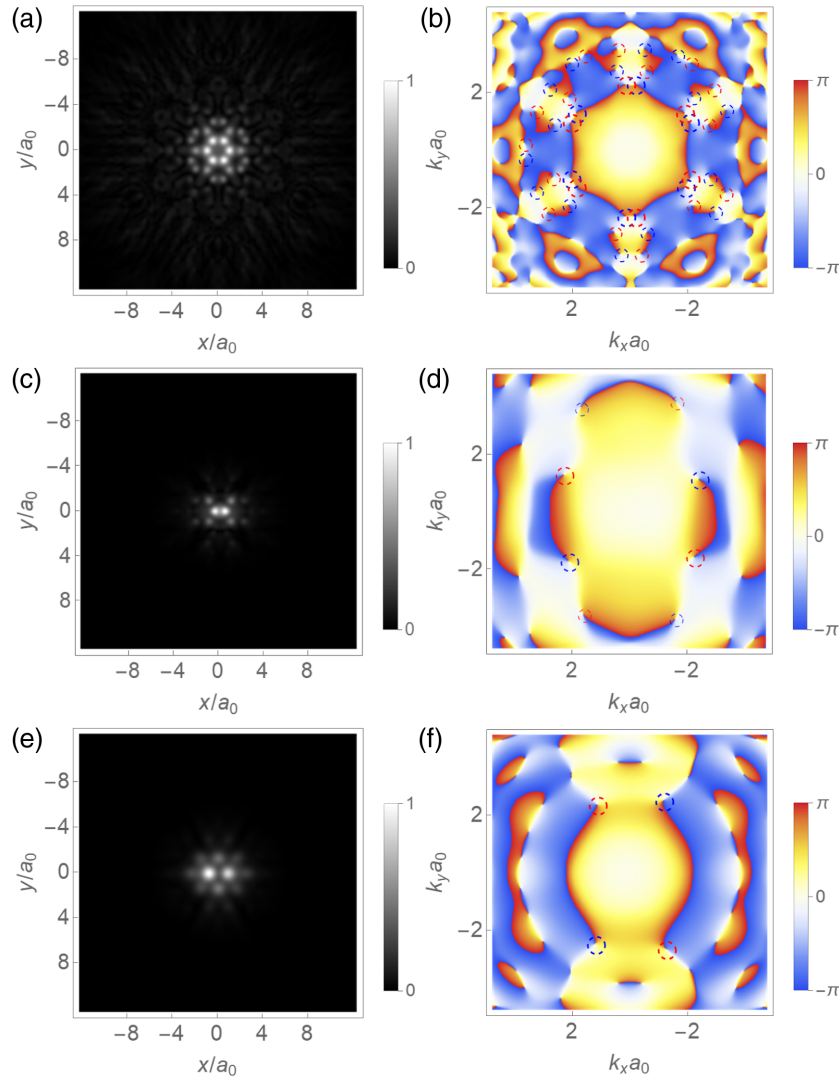
Fig. 4 Numerical solution of the Schrödinger equation showing wave packet expansion in photonic honeycomb and hexagonal lattices with various symmetries of the WFs. (a), (b) Honeycomb lattice, excitation of a single "benzene ring" (C_{6v}): real space probability (a) and momentum space phase (b). (c), (d) The same for a honeycomb lattice, excitation between two sites (C_{2v} symmetry). (e), (f) The same for a topologically trivial hexagonal lattice with C_{2v}-excitation.

We have tested the configurations described above based on differing symmetries experimentally; the corresponding data is presented in Fig. 5. Figures 5(a) and 5(b) show the momentum space interference pattern and the result of phase extraction for the case where the honeycomb lattice was excited at the center of the hexagonal ring, thus providing the C_{6v} symmetry. In accordance with theoretical predictions, this symmetry violates the presence of momentum space vortices at Dirac points. For the case of C_{2v} symmetry in a honeycomb lattice obtained by excitation between two lattice sites, one can observe the two vortex-antivortex pairs; see Figs. 5(c) and 5(d).

The WF of C_{2v} symmetry can be also realized in the hexagonal lattice lacking the sources of Berry curvature. Figures 4(e) and 4(f) show the WF in real space and its phase image in momentum space, which exhibits rectangular vortex patterns very similar to Figs. 4(c) and 4(d).

To test the corresponding configuration experimentally, we have established the required topologically trivial hexagonal lattice, with a lattice constant of $\sim$131 μm, by setting the frequency detunings to $\Delta_1 = -190$ MHz and $\Delta_2 = -100$ MHz, as simulated in Fig. 1(d). The probe beam was focused at the middle point between two lattice sites. Four vortices, composed of two vortex and anti-vortex pairs, appear at the corners of a slightly skewed rectangle, as shown in Figs. 5(e) and 5(f). This indicates that the generation of multiple vortices can still occur in topologically trivial structures, demonstrating that symmetry plays the main role instead of topology.

4 Discussion

Thus one can conclude that Berry curvature sources do not play a key role for generation of vortices in momentum space in the present configuration, but the symmetry does. Fourier transform
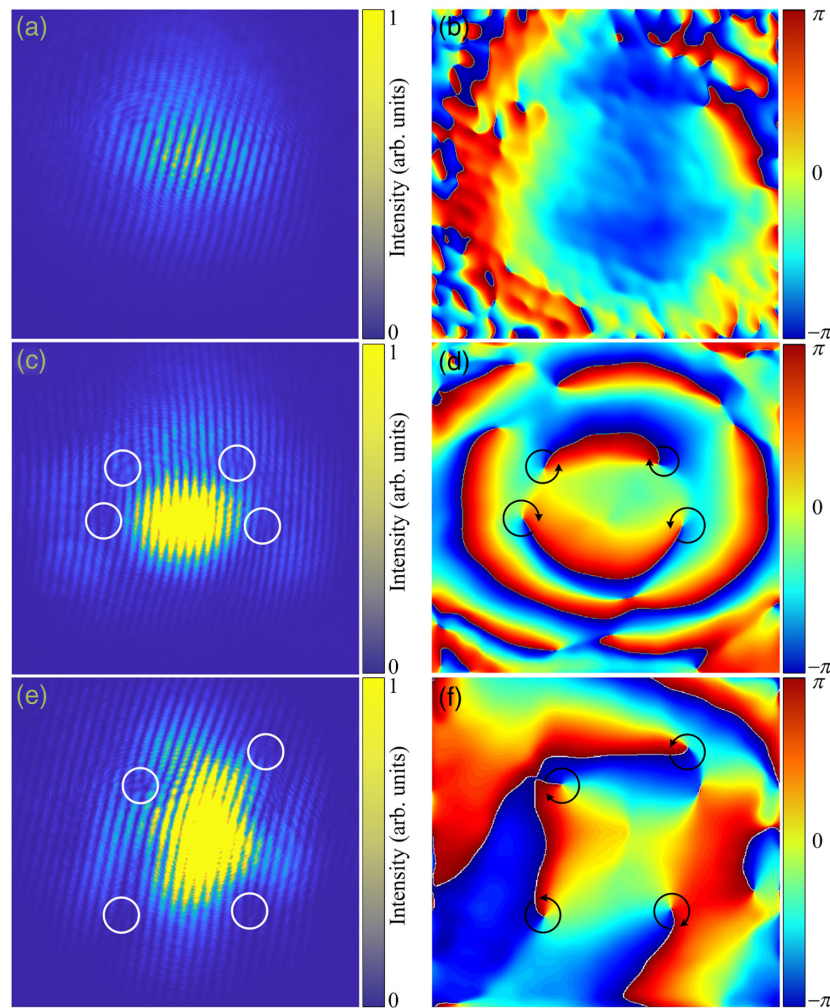
Fig. 5 Phase patterns in momentum space for alternative symmetries and lattices. Panels (a) and (b) demonstrate absence of vortices for the case of C_{6v} symmetry signal in honeycomb lattice. The momentum space interference image shown in panel (a) contains no fork dislocations in fringe pattern and the extracted phase shown in panel (b) also demonstrates no vortex-like phase defects. Panels (c) and (d) show the interference pattern and extracted phase, respectively, for the C_{2v} symmetry signal realized in the honeycomb lattice by excitation between two sites. Panels (e) and (f) are for the interference pattern and extracted phase, respectively, in the case of the C_{2v} symmetry in hexagonal lattice realized experimentally by setting the two-photon detuning −90 MHz.

maps the symmetry of the WF in real space to momentum space. At the same time, the photonic lattices are a very flexible and simple way to implement symmetries that will be inherited by the evolving wave packet. In addition, the lattice defines the size of the wave packet in real space, and also consequently defines the profile of the wave packet in momentum space, including the positions of vortices. The particular symmetry of the WF as well as its radial distribution can be shaped by position and profile of the excitation beam. We benefit from advanced application of discrete nondiffracting beams[34] by usage of real and momentum space equivalence and control of the signal symmetry. Even the simplest Gaussian beams carrying no OAM (cf. Refs. 19, 37, and 38) allow flexible engineering of the WF profile and realization of momentum space vortices with multiple configurations. Moreover, in contrast with, e.g., Refs. 20, 31, and 32, selective addressing sublattice and valley in the honeycomb

lattice are also not needed. The described experimental scheme does not require structured light for probing and dramatically simplifies the techniques for creating vortices employing a honeycomb photonic lattice.

The symmetries were always understood as being absolutely fundamental in physics.[39] While in previous decades the topological invariants have appeared in solid-state physics as something seeming to go beyond symmetries, recent works have started to reestablish their relation to symmetries via the so-called symmetry indicators,[40–43] allowing one to determine the topology from the eigenstates at high symmetry points. Our work makes an important step in this direction, demonstrating that formation of topological defects such as momentum space vortices in periodic potentials is not necessarily determined exclusively by topology of the lattice, while the lattice symmetries can be an origin of complex OAM textures.

Reciprocal space vortices and their pairs can be studied as a part of a global reciprocal space pattern, but they can also be used for reciprocal space engineering of beams for further real-space applications. Indeed, different wave vectors in the reciprocal space correspond to different propagation angles, and the parts of the beam described by different wave vector components split in space while propagating after the vapor cell. This allows one to select a certain region of the reciprocal space and filter away everything else, as has already been done in previous works.[31,33] For example, if three pairs of opposite-sign vortices are formed at the Dirac points (Fig. 2), one can select only a region of wave vectors (propagation angles) corresponding to a given Dirac point with a single vortex. The Fourier transform of this filtered beam from reciprocal to real space necessarily gives a vortex in real space (see, e.g., Ref. 44 as an example of vortex conservation in Fourier conversion), and such vortices have numerous applications,[45] including data encoding,[46] tractor beams,[47] and holographic optical tweezers.[45,48] Generation of multiple vortices in real or momentum space is important for multiplexing[49] and high-angular momentum states.[50] Investigation of vortex pair dynamics is important for studies of quantum turbulence in the framework of point-like vortex gas models[51–55], and appropriate methods are required to create the vortex pairs to trace further evolution. The problem of initial excitation (quantum fluid "stirring") is also important for the studies of quantum turbulence[4–6,56], and the proposed scheme of simultaneous generation of multiple vortices can be beneficial for engineering the initial WF by vortex imprinting.[57,58] Finally, the obtained momentum space phase patterns can serve as starting point for spatial light modulator phase profiles to selectively address the photonic lattice sites in real space.[59]

In conclusion, we have shown the presence of vortices in momentum space aligned in the vicinity of Dirac points in photonic graphene based on the atomic vapor cell with spatially modulated susceptibility after the scattering of a narrow probe beam. This configuration is an analog of the wave packet evolution in honeycomb lattice in the framework of the Schrödinger equation with single-site initial excitation. In the honeycomb lattice, C_{3v} symmetry of the wave packet supports, whereas C_{6v} symmetry cancels, the presence of vortices near the Dirac points. The vortices can exist regardless the topological properties of the lattice. For C_{2v} symmetry WF, vortices also form a rectangular pattern with a lower (mirror reflection) symmetry of the spreading wave packet, both in hexagonal and honeycomb lattices. These results show that the creation of multiple momentum space vortices is strongly linked with the wave-packet symmetry, but not necessarily with the topological nature of the lattice. The resulting pattern of vortices is determined by the product of the probe and the lattice symmetries. Our results provide a novel method to generate well-distinguished vortex arrays in the simplest manner that requires no structured probe light, and reveal the basic rules of how to achieve the desired spatial distribution of vortices by designing the initial symmetry of the lattice and of the probe beam.

Disclosures

The authors declare no conflicts of interest.

Code and Data Availability

Data underlying the results presented in this paper may be obtained from the authors upon reasonable request.

References

1. L. Onsager, "Statistical hydrodynamics," *Il Nuovo Cimento (1943-1954)* **6**(S2), 279–287 (1949).
2. A. A. Abrikosov, "The magnetic properties of superconducting alloys," *J. Phys. Chem. Solids* **2**(3), 199–208 (1957).
3. A. S. Bradley and B. P. Anderson, "Energy spectra of vortex distributions in two-dimensional quantum turbulence," *Phys. Rev. X* **2**(4), 041001 (2012).
4. G. Gauthier et al., "Giant vortex clusters in a two-dimensional quantum fluid," *Science* **364**(6447), 1264–1267 (2019).
5. S. P. Johnstone et al., "Evolution of large-scale flow from turbulence in a two-dimensional superfluid," *Science* **364**(6447), 1267–1271 (2019).
6. S. Koniakhin et al., "2D quantum turbulence in a polariton quantum fluid," *Chaos, Solitons Fractals* **132**, 109574 (2020).
7. I. Carusotto and C. Ciuti, "Quantum fluids of light," *Rev. Mod. Phys.* **85**, 299–366 (2013).
8. K. G. Lagoudakis et al., "Quantized vortices in an exciton–polariton condensate," *Nat. Phys.* **4**(9), 706–710 (2008).
9. S. Koniakhin et al., "Stationary quantum vortex street in a driven-dissipative quantum fluid of light," *Phys. Rev. Lett.* **123**(21), 215301 (2019).
10. F. Claude et al., "Taming the snake instabilities in a polariton superfluid," *Optica* **7**(12), 1660–1665 (2020).
11. D. Caputo et al., "Topological order and thermal equilibrium in polariton condensates," *Nat. Mater.* **17**, 145–151 (2018).
12. A. Kavokin, G. Malpuech, and M. Glazov, "Optical spin Hall effect," *Phys. Rev. Lett.* **95**(13), 136601 (2005).
13. S. Koniakhin et al., "Topological turbulence in spin-orbit–coupled driven-dissipative quantum fluids of light generates high-angular-momentum states," *Europhys. Lett.* **133**(6), 66001 (2021).
14. Y. G. Rubo, "Half vortices in exciton polariton condensates," *Phys. Rev. Lett.* **99**(10), 106401 (2007).
15. S. Dufferwiel et al., "Spin textures of exciton-polaritons in a tunable microcavity with large TE-TM splitting," *Phys. Rev. Lett.* **115**(24), 246401 (2015).
16. C. Bena and G. Montambaux, "Remarks on the tight-binding model of graphene," *New J. Phys.* **11**(9), 095003 (2009).
17. J. Fuchs et al., "Topological Berry phase and semiclassical quantization of cyclotron orbits for two dimensional electrons in coupled band models," *Eur. Phys. J. B* **77**(3), 351–362 (2010).
18. L.-K. Lim, J.-N. Fuchs, and G. Montambaux, "Geometry of Bloch states probed by Stückelberg interferometry," *Phys. Rev. A* **92**(6), 063627 (2015).

19. X. Liu et al., "Universal momentum-to-real-space mapping of topological singularities," *Nat. Commun.* **11**(1), 1586 (2020).
20. D. Song et al., "Valley vortex states and degeneracy lifting via photonic higher-band excitation," *Phys. Rev. Lett.* **122**(12), 123903 (2019).
21. Y. Zhang et al., "Observation of polarization vortices in momentum space," *Phys. Rev. Lett.* **120**(18), 186103 (2018).
22. B. Wang et al., "Generating optical vortex beams by momentum-space polarization vortices centred at bound states in the continuum," *Nat. Photonics* **14**(10), 623–628 (2020).
23. K. Yang, Y. Wang, and C.-X. Liu, "Momentum-space spin antivortex and spin transport in monolayer pb," *Phys. Rev. Lett.* **128**(16), 166601 (2022).
24. P. Vaity and L. Rusch, "Perfect vortex beam: Fourier transformation of a Bessel beam," *Opt. Lett.* **40**(4), 597–600 (2015).
25. X. Qiu et al., "Optical vortex copier and regenerator in the Fourier domain," *Photonics Res.* **6**(6), 641–646 (2018).
26. V. Kotlyar, A. Kovalev, and A. Porfirev, "Vortex astigmatic Fourier-invariant Gaussian beams," *Opt. Express* **27**(2), 657–666 (2019).
27. B. Muminov and L. T. Vuong, "Fourier optical preprocessing in lieu of deep learning," *Optica* **7**(9), 1079–1088 (2020).
28. J. Gea-Banacloche et al., "Electromagnetically induced transparency in ladder-type inhomogeneously broadened media: theory and experiment," *Phys. Rev. A* **51**(1), 576–584 (1995).
29. Z. Zhang et al., "Angular-dependent Klein tunneling in photonic graphene," *Phys. Rev. Lett.* **129**(23), 233901 (2022).
30. Z. Zhang et al., "Observation of edge solitons in photonic graphene," *Nat. Commun.* **11**, 1902 (2020).
31. Z. Zhang et al., "Particlelike behavior of topological defects in linear wave packets in photonic graphene," *Phys. Rev. Lett.* **122**(23), 233905 (2019).
32. D. Song et al., "Unveiling pseudospin and angular momentum in photonic graphene," *Nat. Commun.* **6**(1), 6272 (2015).
33. Z. Zhang et al., "Spin-orbit coupling in photonic graphene," *Optica* **7**, 455 (2020).
34. M. Boguslawski, P. Rose, and C. Denz, "Increasing the structural variety of discrete nondiffracting wave fields," *Phys. Rev. A* **84**(1), 013832 (2011).
35. S. V. Koniakhin, "Ratchet effect in graphene with trigonal clusters," *Eur. Phys. J. B* **87**(9), 216 (2014).
36. C. Dutreix et al., "Measuring the Berry phase of graphene from wavefront dislocations in Friedel oscillations," *Nature* **574**(7777), 219–222 (2019).
37. T. Boulier et al., "Vortex chain in a resonantly pumped polariton superfluid," *Sci. Rep.* **5**(1), 9230 (2015).
38. D. Choi et al., "Observation of a single quantized vortex vanishment in exciton-polariton superfluids," *Phys. Rev. B* **105**(6), L060502 (2022).
39. L. D. Landau and E. M. Lifshitz, *Mechanics*, Butterworth-Heinemann (1976).
40. L. Fu and C. L. Kane, "Topological insulators with inversion symmetry," *Phys. Rev. B* **76**(4), 045302 (2007).
41. H. C. Po, A. Vishwanath, and H. Watanabe, "Symmetry-based indicators of band topology in the 230 space groups," *Nat. Commun.* **8**(1), 50 (2017).
42. Z. Song et al., "Quantitative mappings between symmetry and topology in solids," *Nat. Commun.* **9**(1), 3530 (2018).
43. F. Tang et al., "Efficient topological materials discovery using symmetry indicators," *Nat. Phys.* **15**(5), 470–476 (2019).
44. A. Chong et al., "Generation of spatiotemporal optical vortices with controllable transverse orbital angular momentum," *Nat. Photonics* **14**(6), 350–354 (2020).
45. D. G. Grier, "A revolution in optical manipulation," *Nature* **424**(6950), 810–816 (2003).
46. M. Erhard et al., "Twisted photons: new quantum perspectives in high dimensions," *Light Sci. Appl.* **7**(3), 17146 (2018).
47. D. Gao et al., "Optical manipulation from the microscale to the nanoscale: fundamentals, advances and prospects," *Light Sci. Appl.* **6**(9), e17039 (2017).
48. M. Padgett and R. Bowman, "Tweezers with a twist," *Nat. Photonics* **5**(6), 343–348 (2011).
49. J. Wang et al., "Terabit free-space data transmission employing orbital angular momentum multiplexing," *Nat. Photonics* **6**(7), 488–496 (2012).
50. G. Spektor et al., "Orbital angular momentum multiplication in plasmonic vortex cavities," *Sci. Adv.* **7**(33), eabg5571 (2021).
51. Y. B. Pointin and T. Lundgren, "Statistical mechanics of two-dimensional vortices in a bounded container," *Phys. Fluids (1994)* **19**(10), 1459–1470 (1976).
52. J. H. Kim, W. J. Kwon, and Y.-I. Shin, "Role of thermal friction in relaxation of turbulent Bose-Einstein condensates," *Phys. Rev. A* **94**(3), 033612 (2016).
53. M. T. Reeves et al., "Enstrophy cascade in decaying two-dimensional quantum turbulence," *Phys. Rev. Lett.* **119**(18), 184502 (2017).
54. X. Yu and A. S. Bradley, "Emergent non-eulerian hydrodynamics of quantum vortices in two dimensions," *Phys. Rev. Lett.* **119**(18), 185301 (2017).
55. R. N. Valani, A. J. Groszek, and T. P. Simula, "Einstein–Bose condensation of Onsager vortices," *New J. Phys.* **20**(5), 053038 (2018).
56. R. Panico et al., "Onset of vortex clustering and inverse energy cascade in dissipative quantum fluids," *Nat. Photonics* **17**(5), 451–456 (2023).
57. T. Simula, M. J. Davis, and K. Helmerson, "Emergence of order from turbulence in an isolated planar superfluid," *Phys. Rev. Lett.* **113**(16), 165302 (2014).
58. H. Salman and D. Maestrini, "Long-range ordering of topological excitations in a two-dimensional superfluid far from equilibrium," *Phys. Rev. A* **94**(4), 043642 (2016).
59. O. Jamadi et al., "Reconfigurable photon localization by coherent drive and dissipation in photonic lattices," *Optica* **9**(7), 706–712 (2022).

Feng Li is a professor at Xi'an Jiaotong University, China. He received the bachelor's and master's degrees at Tianjin University, China, in 2006 and 2008, respectively. He obtained his PhD at CNRS and the University of Nice Sophia Antipolis, France, in 2013, supported by the European Marie Curie ITN project CLERMONT4. Subsequently, he worked as a research associate at the University of Sheffield, United Kingdom, from January 2014 to May 2017. He joined Xi'an Jiaotong University as a professor in June 2017, with a main research interest in light–matter interaction in microcavities and micro/nanostructures.

Sergei V. Koniakhin received his BS and MS degrees in Peter the Great St.Petersburg Polytechnic University in 2012 and worked as a junior researcher at Ioffe Institute, St.Petersburg, Russia from 2010 to 2015; he defended his PhD thesis in 2016. From 2015 to 2021, he worked as a researcher and senior researcher in Zhores Alferov University, St. Petersburg. From 2017 to 2020, he was a PhD student at Institut Pascal, Clermont-Ferrand, France. He became a Young Scientist Fellowship Team Leader at the Physics of Complex Systems Center, Institute for Basic Science, Daejeon, Republic of Korea starting in 2021.

Anton V. Nalitov obtained his master's degree in condensed matter physics from Saint-Petersburg Academic (Zhores Alferov) University, Russia, in 2012, and his PhD from Université Blaise Pascal, Clermont-Ferrand, France, in 2015. His professional path includes Ioffe Institute, University of Southampton, University of Iceland, and University of Wolverhampton. Currently, he is a senior research assistant at Abrikosov Center for Theoretical Physics, Moscow Institute of Physics and Technology.

Evgeniia Cherotchenko obtained her master's degree from Peter the Great St.Petersburg Polytechnic University in 2012 and her PhD from the University of Southampton in 2017. Her research experience includes working in ITMO University and currently she conducts her research in Ioffe Institute of the Russian Academy of Sciences.

Dmitry D. Solnyshkov is a professor at the University Clermont Auvergne, France. He wrote his PhD thesis in France, in 2007, became an assistant professor in 2008, and obtained his HDR (second thesis) in 2012, to become a full professor in 2019. He was a junior member of Institut Universitaire de France in 2017 to 2022. He is a theoretician working on Bose–Einstein condensation, quantum fluids, strong light–matter coupling, and topology.

Guillaume Malpuech is CNRS senior researcher at the Institut Pascal in Clermont Ferrand, France. He received his PhD in 2001 from the University Blaise Pascal and became CNRS researcher at the Institut Pascal in 2002. He is a theoretician working on exciton-polaritons, quantum fluids of light, and topological photonics. His major contributions are the proposals of room temperature polariton lasers, spin-orbit coupling of light based on TE-TM splitting, polariton Chern insulators, topological lasers, and quantum geometric tensor measurement.

Zhaoyang Zhang received his doctoral degree in electronic science and technology from Xi'an Jiaotong University. He is currently a professor at the School of Electronic Science and Engineering at Xi'an Jiaotong University. His research focuses mainly on atomic physics and nonlinear optics.

Biographies of the other authors are not available.